AIAA 80-1089R

Experimental Investigation of Endwall Profiling in a Turbine Vane Cascade

F. C. Kopper* and R. Milano†
United Technologies Corporation, East Hartford, Conn.
and
M. Vanco‡
NASA Lewis Research Center, Cleveland, Ohio

Measurements of surface static pressures, flow total pressure loss, and exit air angle were obtained for two linear cascades to establish the effects of endwall profiling. Testing was conducted at an isentropic exit Mach number of 0.85. One cascade was fabricated with planar endwalls while the other had one planar and one profiled endwall. Both cascades utilized the same high pressure turbine inlet guide vane section. It was found that in terms of full passage loss the profiled endwall cascade has the superior performance. The secondary loss results obtained are reasonably well predicted by correlations developed from incompressible flow testing of similar configurations. Inviscid flow and boundary layer calculations are compared with the test data and, overall, the agreement is found to be good. Use of the results for design purposes is briefly discussed.

Nomenclature

BX = airfoil axial chord
C = airfoil chord
C_L = lift coefficient $= 2S/C(\cot\alpha_1 + \cot\alpha_2)\sin\bar{\alpha}$
h = airfoil exit span
M = Mach number
P = static pressure
P_T = inlet freestream total pressure
ΔP_T = change in total pressure relative to inlet freestream
Q = exit flow dynamic head $= \frac{1}{2}\rho U^2$
Re_c = Reynolds number based on C and exit conditions
S = cascade pitch
U = velocity
u' = rms value of velocity fluctuation in the streamwise direction
X, Y = Cartesian coordinates where x is parallel to turbine axis
Y_{SG} = gross secondary loss coefficient $= \Delta P_T/Q$
Z = blade aerodynamic loading coefficient

$$= \left(\frac{C_L}{S/C}\right)^2 \frac{\sin^2\alpha_2}{\sin^3\bar{\alpha}}$$

α_1 = inlet freestream air angle measured from tangential (see Fig. 1)
α_2 = measured mass weighed pitch average exit yaw angle (angle in plane of endwalls) measured from tangential (see Fig. 1)
$\bar{\alpha}$ = mean air angle $= \cot^{-1}[(\cot\alpha_1 - \cot\alpha_2)/2]$
β_1 = inlet blade angle measured from tangential
δ^* = boundary-layer displacement thickness
θ = boundary-layer momentum thickness
ρ = fluid density

Presented as Paper 80-1089 at the AIAA/SAE/ASME 16th Joint Propulsion Conference, Hartford, Conn., June 30-July 2, 1980; submitted Sept. 9, 1980; revision received March 18, 1981.

*Project Engineer, Pratt & Whitney Aircraft Group, Commercial Products Division.
†Analytical Engineer, Pratt & Whitney Aircraft Group, Commercial Products Division.
‡Project Engineer, Energy Efficient Engine Project Office.

Introduction

THE cost of fuel is projected to continue rising at substantial rates. This fact makes it imperative that future aircraft gas turbine engines be designed to achieve the highest possible efficiency. In the high pressure turbine, profiling of the endwall(s) of the inlet guide vane holds promise for achieving improved performance through the reduction of secondary losses. Deich et al.[1] and Ewen et al.[2] both report achieving increases in efficiency in rotating rigs attributed to endwall profiling.

Previous research in the area of endwall profiling was conducted by Morris and Hoare,[3] who investigated a linear cascade fitted with several different endwall geometries. This testing was conducted at an exit Mach number in the incompressible range and at a Reynolds number about an order of magnitude below that of typical commercial engine service conditions. Also, exit air angle data were not obtained, so that mass averaged losses could not be properly determined at the measurement plane.

The objective of the testing being reported in this paper was to obtain data which would allow establishing the performance benefit of endwall profiling when applied to high turning inlet guide vanes projected for use in energy efficient engines of the future. All testing was conducted at a Reynolds number of 1.8×10^6 and an isentropic exit Mach number of 0.85 which are typical of commercial engine altitude cruise conditions. Data obtained include airfoil and endwall static pressure distributions, flow total pressure loss and exit flow velocity and angle.

A further objective was to employ the data to assess the accuracy of analytical methods and to gain a physical understanding of the effect of endwall profiling on the intrapassage flow. These methods range from secondary loss correlations to the numerical modeling of the three-dimensional inviscid flowfield.

The results obtained from the profiled endwall cascade demonstrated a 17% reduction of the full passage mass averaged loss relative to the planar endwall configuration. A major part of the improvement achieved resulted from a reduction of the secondary loss on the planar wall side of the cascade. The secondary loss correlation of Morris and Hoare was found to yield a reasonably good prediction of the area averaged data. Airfoil and endwall static pressure data obtained for the planar wall cascade was very well predicted by a

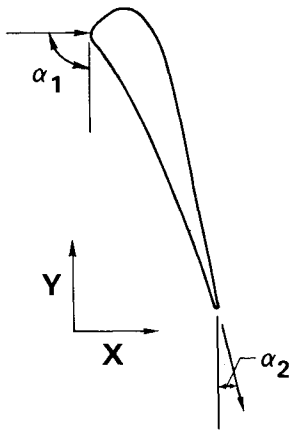

Fig. 1 Vane section.

two-dimensional potential flow computation. Static pressure data for the profiled wall cascade was well predicted by a three-dimensional time-marching method.

Experimental Apparatus and Procedure

Description of Cascades

Two linear cascades were employed in the program conducted. One cascade was fabricated with planar endwalls and was used to obtain baseline data. The second cascade was fabricated with one planar endwall and one endwall profiled in the axial direction. The latter simulates a high pressure turbine inlet guide vane configuration where the outer endwall is profiled as a surface of revolution.

Both cascades utilized the same airfoil section as shown in Fig. 1, which had a chord C of 9.017 cm (3.550 in.) and inlet blade angle β_1 of 90 deg. In addition, both cascades were constructed with equal pitches of 8.467 cm (3.333 in.) and equal exit aspect ratio h/C of 0.513. The planar wall cascade held span h at 4.623 cm (1.820 in.) from inlet to exit, whereas the profiling of the profiled endwall cascade resulted in a larger inlet span of 5.580 cm (2.197 in.). The contour of the profiled endwall is shown in Fig. 2. Airfoils in the planar wall cascade were rotated open slightly to provide equal gaging areas and approximately equal exit air angles for both cascades, thus permitting a one-to-one comparison between cascades.

Because of tunnel constraints both cascades were limited to three airfoils (three pitches). An infinite cascade flowfield was approximated for this configuration by contouring the sidewalls to match the applicable streamline of the flow as established by a compressible potential flow computation. These sidewalls were made adjustable to permit fine tuning of the cascades to achieve periodicity when installed in the tunnel.

Both cascades were provided with static pressure tappings, with the profiled wall cascade being more extensively instrumented to permit assessment of the three-dimensional behavior of the flowfield. Airfoils for both cascades were instrumented along three span locations. In addition, the profiled wall cascade airfoils included one line of tappings lying close to and following the wall profile (see Fig. 2). One endwall of the planar wall cascade was instrumented to obtain pressure data across the passage. Both endwalls of the profiled wall cascade were instrumented in this manner.

Experimental Facility

Testing was conducted in a steady flow cascade wind tunnel facility. In this facility, airflow is provided to the test section upstream plenum by an axial flow compressor driven by a small gas turbine. In the plenum chamber the flow passes through a honeycomb flow straightener and fine mesh screens before being contracted through a rectangular bellmouth to a 50.8 cm (20 in.) long, 7.62×25.4 cm^2 (3×10 in.^{2}) cross-section cascade approach duct. Variable thickness endwall plates were employed to further reduce the width of the duct to match the inlet span of a cascade. After passing through the cascade the air discharges to a large chamber which is maintained at atmospheric pressure.

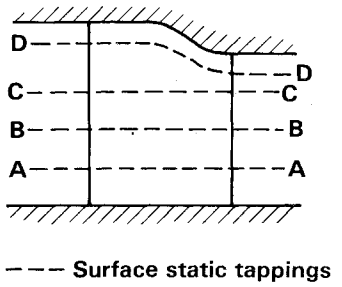

Fig. 2 Profiled endwall contour.

A biplanar grid comprised of 2.38 mm (3/32 in.) square bars with a mesh spacing of 12.7 mm (½ in.) was placed in the approach duct 43.2 cm (17 in.) upstream of the cascade to increase the turbulence in the flow, thus preventing problems of flow separation within the cascade. For this configuration the correlation of Baines and Peterson[4] predicts a freestream turbulence level u'/U of 2.7% at the entrance to the cascade. Hot wire measurements were taken at this location (without a span reducing sideplate installed) at a Mach number of 0.1 corresponding to that encountered in the cascade testing. The measured value of 2.6% u'/U is in excellent agreement with the correlation. Installation of the span reducing sideplates employed in the testing produces an area contraction ratio of approximately 1.5 immediately downstream of the grid which will cause a reduction of freestream turbulence into the cascade. Based on the theory of Batchelor,[5] this contraction is calculated to reduce the intensity of the turbulence from 2.6% to approximately 1.8%.

Sidewall boundary-layer measurements were taken at a location in the approach duct 2.54 cm (1.0 in.) in front of the leading edge plane of the cascade. Data were obtained for a range of Mach numbers and Reynolds numbers covering those encountered in the testing. Integral boundary-layer parameters were evaluated for the measured velocity profiles, and were found to be in reasonably good agreement with those calculated using a formulation for the development of a zero pressure gradient fully turbulent boundary layer originating at the grid.[6] Interpolation between the measured data was subsequently used to obtain the inlet displacement and momentum thicknesses for the two cascades at their respective testpoint conditions.

Data Acquisition

To assess cascade performance, wake traverses were made in a plane 10.16 mm (0.4 in.) axially downstream of the trailing edge plane. A five port combination probe was used to obtain measurements of total pressure, static pressure, and pitch and yaw angles over the traverse plane. This probe had a stem diameter of 3.97 mm (5/32 in.) and a conical tip of 70 deg total included angle. Close to the endwalls a boundary layer type probe was employed. This probe consisted of three 0.559 mm (0.022 in.) diameter capillary tubes flattened to a height of 0.279 mm (0.011 in.), and brazed in parallel. The two side tubes were cut off at a 45 deg angle. Both probes were run in a free jet calibration facility to develop calibration curves for total pressure, static pressure, yaw angle, and pitch angle (5 port combination probe only). This calibration was conducted at approximately the same unit Reynolds number as the cascade exit flow and over the range of Mach numbers and angles required for the testing.

The above probes were used in conjunction with a traverse system consisting of a probe drive mechanism and controller, pressure transducers and associated dead weight calibrators and data recording equipment. In acquiring data, the probes

Table 1 Test conditions

	Planar endwall cascade	Profiled endwall cascade
Isentropic exit Mach no.	0.849	0.845
Upstream air angle, α_1	90 deg	90 deg
Upstream Mach no.	0.109	0.091
Reynolds no., Re_c	1.68×10^6	1.89×10^6
Upstream total pressure, P_T	1.606 bar (23.29 psia)	1.622 bar (23.53 psia)
Total temperature	347 K (624°R)	319 K (574°R)
Displacement thickness, δ^* [a]	0.117 cm (0.046 in.)	0.125 cm (0.049 in.)
Momentum thickness [a]	0.089 cm (0.035 in.)	0.091 cm (0.036 in.)
Momentum thickness Reynolds no. [a]	2895	2466
δ^*/C	0.0130	0.0138

[a] Inlet endwall boundary layer.

were traversed in the pitchwise direction at a constant span height taking measurements at 1.52 mm (0.060 in.) increments. Yaw angles (angles in plane parallel to endwalls) were obtained by nulling the probe aerodynamically to within one degree and then employing the calibration curves. It should be noted that the probe drive axis of rotation passed through the tip of the probe. Pitch angles were obtained for the five port combination probe through the calibration curves. Each full passage exit survey nominally consisted of 35 pitchwise traverses covering the full span of the cascade with these traverses being more concentrated near the endwalls.

Test Conditions

Full passage exit plane surveys and surface static pressure data were obtained for each cascade at a nominal exit isentropic Mach number of 0.85. Table 1 presents the measured test conditions for each cascade along with the associated inlet sidewall boundary-layer parameters. These conditions are representative of altitude cruise conditions for the turbine design in which the vane section would be employed.

Experimental Uncertainty

Experimental uncertainties for the results obtained are estimated to be $\pm 0.02 P/P_T$ for surface static data; ± 0.4 deg for gap average mass weighed exit air angle (α_2) and ± 0.02 for the gap average exit Mach number. Mass averaged total pressure loss results are estimated to be accurate within $+5\%$ to -8% $\Delta P_T/P_T$ inside the profile loss region and $+10\%$ to -14% $\Delta P_T/P_T$ inside the secondary loss region.

Results and Discussion

Flow Visualization

Surface flow visualizations were conducted for both cascades to assess the behavior of the limiting streamlines and to establish if any flow separation problems existed. These flow visualizations were made by applying a mixture of lampblack and oil to the airfoil and endwall surfaces and subsequently operating the cascade tunnel at test point conditions for approximately one minute. Figure 3a presents a photograph of the flow visualization achieved for the planar wall cascade viewed from upstream, and Fig. 3b shows the profiled wall cascade viewed from downstream. Both

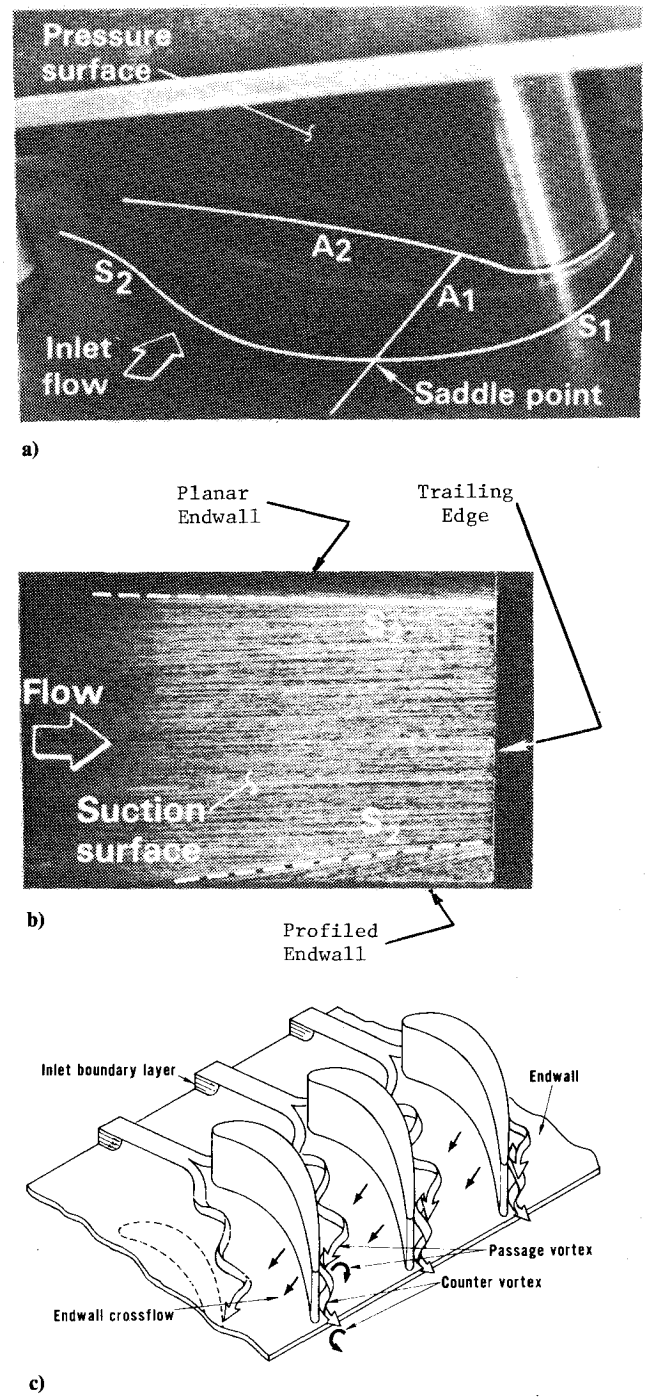

Fig. 3 Cascade surface flow visualizations: a) flow visualization of planar wall cascade viewed from upstream; b) flow visualization of profiled wall cascade viewed from downstream; c) schematic representation of cascade secondary flow.

cascades exhibited the same qualitative features detailed by Langston et al.[7] in testing a large scale cascade of turbine airfoils which since have been substantiated by Carrick[8] and Marchal and Sieverding.[9]

The features of the three-dimensional separation at the cascade inlet are shown in Fig. 3a. Here the inlet boundary layer separates along lines S_1 and S_2 to form a "horseshoe vortex" containing the low momentum boundary layer fluid (see Fig. 3c). The leg corresponding to S_1 gets wrapped around the suction side of the airfoil to form what has been called the "counter vortex," while the leg corresponding to S_2 moves toward the suction side of the adjacent airfoil to form the "passage vortex." The new boundary layer formed within the region bounded by separation line S_2 and at-

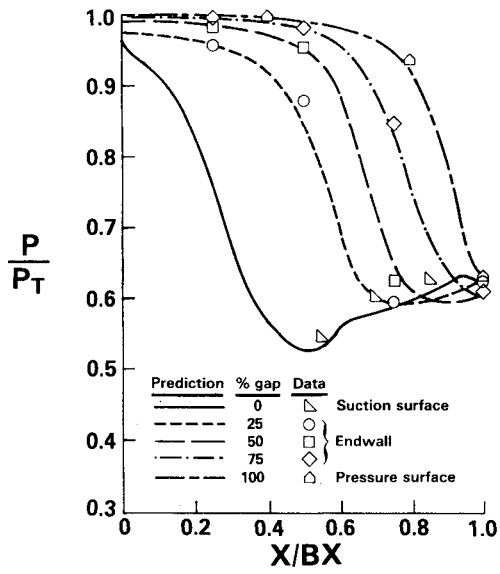

Fig. 4 Comparison of planar wall cascade data with potential flow computation of Caspar et al.

tachment lines A_1 and A_2 is swept toward the suction side of the adjacent airfoil by the cross-channel pressure gradient. This low momentum fluid subsequently contributes to the growth of the passage vortex making it the dominant feature of cascade secondary flow. Toward the rear of the airfoil, separation line S_2 moves onto the suction surface of the adjacent airfoil, as can be seen in Fig. 3b of the cascade exit plane.

From the flow visualizations of the rear of the suction surface, the planar endwall cascade features were seen to be very symmetric about midspan, while the profiled wall cascade (Fig. 3b) was seen to exhibit slight asymmetry, which is to be expected. In particular, the passage vortex separation line alongside the planar endwall was found to be closer to the endwall than that on the profiled wall side; approximately 5.08 mm (0.20 in.) at the trailing edge for the planar side vs 6.35 mm (0.25 in.) for the profiled side. This distance was found to be approximately 6.35 mm (0.25 in.) for both sides of the planar wall cascade.

Pressure Distribution Analysis

Static pressure data were obtained on the airfoils and endwalls of both the planar wall and the profiled wall cascades. Airfoil-to-airfoil comparison of static pressure data

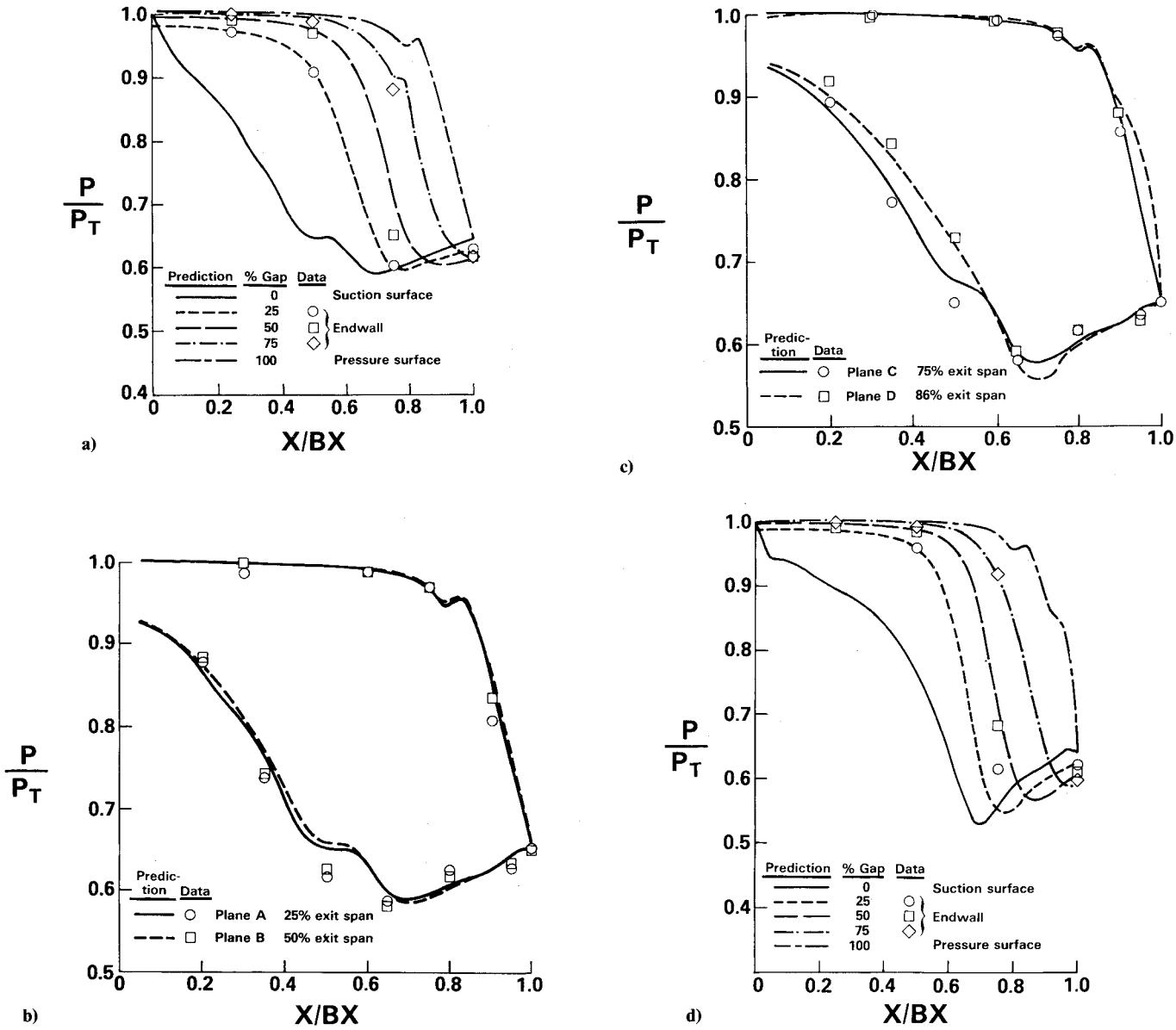

Fig. 5 Comparison of profiled wall cascade data with time-marching computation of Denton: a) planar endwall; b) planes A and B (see Fig. 2); c) planes D and E (see Fig. 2); and d) profiled endwall.

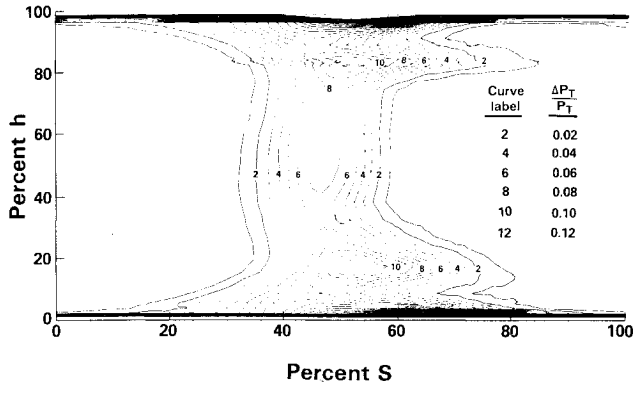

Fig. 6 Loss contour plot for planar wall cascade.

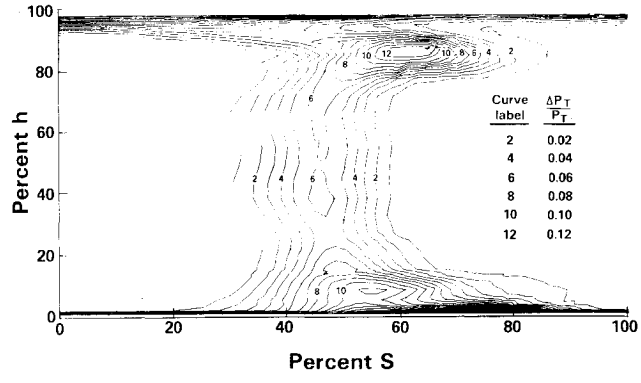

Fig. 7 Loss contour plot for profiled wall cascade.

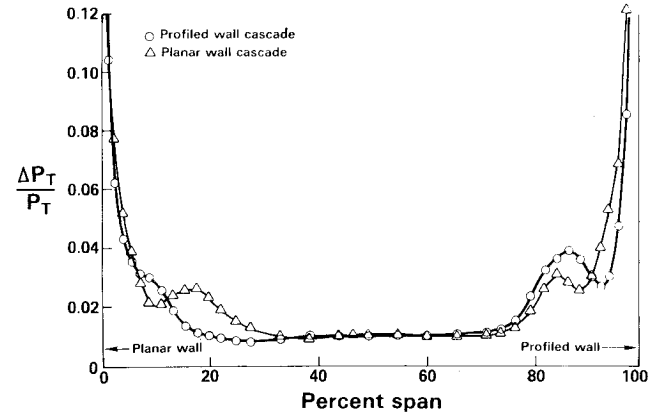

Fig. 8 Spanwise distribution of total pressure loss.

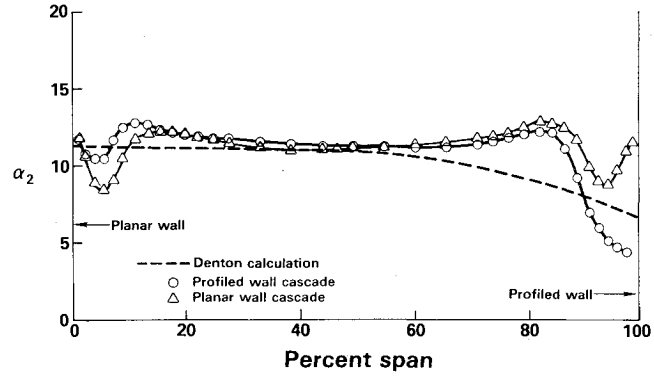

Fig. 9 Spanwise distribution of exit yaw angle.

was used to establish periodicity within the cascade before any data was acquired. Both the planar wall and profiled wall cascades showed excellent agreement in comparing pressure readings at corresponding locations on each airfoil indicating excellent periodicity was achieved.

Static pressure measurements obtained for the planar wall cascade appear in Fig. 4, along with the results of a two-dimensional compressible potential flow calculation. This calculation was performed employing the method of Caspar et al.[10] which solves the steady compressible potential flow equations in the physical plane using a finite area formulation. The solution of the potential flow equations requires defining both inlet and exit flow boundary conditions. The prediction shown in Fig. 4 used measured inlet and exit conditions and is seen to exhibit good agreement with the data. Since the prediction stems from an inviscid formulation, a trailing edge stagnation point is calculated which would appear as a spike at the trailing edge in the pressure distribution. To eliminate this, the predicted pressure distribution shown has been faired to the measured base pressure over the last 5% axial chord.

The asymmetric geometry of the profiled wall cascade is expected to produce a three-dimensional flowfield; as a consequence, the method of Caspar et al. would no longer be applicable. Denton[11,12] has proposed a procedure employing the time-marching concept to calculate the three-dimensional inviscid flowfield in an airfoil passage. In this approach the governing equations of motion (Euler equations) are considered in integral form. The flowfield is broken up into a series of finite volumes and the governing equations reduced to a series of conservation relations for each of these volumes.

Figures 5a-d present comparisons between measured airfoil and endwall static pressure data and a prediction employing the method of Denton. In executing this calculation the measured downstream static pressure was imposed as the downstream boundary condition. Overall, the agreement between prediction and data is seen to be good.

Measured Cascade Performance

The wake traverse data taken were used to determine cascade performance in terms of total pressure loss and exit air angles. From these data contour plots of total pressure loss in the exit plane were produced. Figure 6 shows the loss contours for the planar wall cascade over one pitch. The airfoil wake may be readily seen as near parallel contours running spanwise within the profile loss region of span. Nearer the endwalls the regular pattern is disrupted by the secondary flows with the passage vortex appearing in the contour plots as the circular region of high pressure loss near the endwalls.

Closer to the endwalls the boundary layers which develop within the passage produce a sharp increase in total pressure loss. The pressure loss contour plot for the profiled wall cascade shown in Fig. 7 exhibits similar features; however, the high loss region (passage vortex) on the planar wall side is seen to lie somewhat closer to the endwall than on the profiled wall side. This is consistent with the suction surface separation lines observed in the flow visualizations.

The spanwise distribution of mass averaged total pressure loss for both cascades is shown in Fig. 8. The most notable feature for the profiled wall cascade is the apparent lack of the total pressure loss peak due to the passage vortex on the planar wall side. This can be explained by the fact that the vortex on this side lies closer to the endwall, and pitchwise integration of loss data merges this loss region into that of the endwall boundary layer.

Yaw angle data were mass averaged in the pitchwise direction in the same manner as the pressure loss data. The yaw angle distribution of the planar wall cascade is presented in Fig. 9, and is seen to show good symmetry about midspan.

The passage vortices near the endwalls result in a region of first underturning and then overturning as one proceeds from midspan across the vortices toward the endwalls. Closer to the endwalls the flow is seen to again exhibit decreased turning.

This is attributed to the suction side leg of the leading edge vortex ("counter vortex," see Fig. 3c) which has been observed in large scale experiments.

The spanwise distribution of yaw angle for the profiled wall cascade is also presented in Fig. 9 and shows that to a very good approximation the same overall turning was achieved for both cascades. These data show the same general trends discussed above with the exception that the flow on the profiled wall side is seen to exhibit appreciable overturning. This trend is predicted, in an average sense, by the three-dimensional time-marching calculation also shown on Fig. 9, and suggests that the "inviscid" contribution to the behavior of the endwall flow is appreciable. Worthy of note is the fact that the flow on the planar endwall side of the profiled cascade exhibits less deviation from the midspan value than the planar wall cascade. A further discussion of the cascade secondary flows and losses will be deferred to a later section.

Profile Loss Analysis

Because of the strong overall acceleration experienced by the flow in the cascades under investigation, it would be expected that even at the relatively low aspect ratio of about 0.5 the midspan region would be reasonably two-dimensional in nature and, therefore, be amenable to two-dimensional analytical methods.

The approach taken in making a prediction of the midspan total pressure loss was to employ the results from the pressure distribution calculations discussed earlier to execute two-dimensional boundary-layer computations for both the pressure and suction surfaces. Here it should be pointed out that for the profiled wall cascade the pressure distribution remains, to a good approximation, constant over 75% of the span on the planar wall side justifying the approach. A wake mixing calculation was subsequently utilized to mix out the boundary layers and account for the finite thickness of the airfoil trailing edge.

The boundary layer code used was that of McNally,[13] which is a two-dimensional integral formulation including the effects of compressibility. The laminar formulation is that of Cohen and Reshotko[14] and the turbulent formulation that of Sasman and Cresci[15] with a correlation being added to the code to predict the laminar-to-turbulent transition point for flows having appreciable freestream turbulence. Mixing out of the boundary layers at the trailing edge to a homogeneous flow condition downstream was executed employing the formulation of Stewart.[16]

Boundary-layer calculations for both cascades predicted that transition occurs on the suction surface slightly downstream of the start of the adverse pressure gradient. The pressure surface in both cases was predicted to remain laminar to the trailing edge. The predicted total pressure loss for both cascades using the above procedure was found to be within 10% of the values obtained by mixing out the respective wake traverse data to uniform properties through the application of the equations of conservation of mass and momentum.[17]

Secondary Loss Analysis

The wake traverse plane was chosen at a distance downstream of the cascade where, from past experience, it is considered that the flow is sufficiently mixed out to permit a reasonable assessment of the secondary losses. In addition, the test results were analyzed on both an area averaged and a mass averaged basis. Secondary loss results were obtained by the conventional approach of subtracting the profile loss from the full passage loss. Profile loss was evaluated by using the appropriate mass or area averaged loss over 20% of the span about midspan. The resulting values for secondary loss thus include the contributions from the inlet boundary layer, the passage endwall boundary layer, and the interaction between the endwall and airfoil boundary layers.

Table 2 presents the results for both the planar wall and the profiled wall cascades in terms of mass averaged and area averaged values. These results are presented for each half span, as well as over the full passage, in order to bring out the effect of profiling one endwall. In general, the results show the secondary loss to account for over half the total loss. It should be pointed out that the area averaged loss does not take account of the reduced mass flow in regions of higher total pressure loss, and as a consequence the area averaged losses are somewhat higher than the mass averaged values.

Comparison of the mass averaged data for the two cascades shows the profiled wall cascade to have 17% less full passage loss. Since the measured profile losses were approximately equal for these cascades, this improvement was in the secondary losses (approximately 30% reduction). Comparison of the data for each half span shows that most (approximately 65%) of this improvement occurred on the planar wall half with improvements shown on both halves. Area averaging of the data also shows a substantial reduction in secondary loss for the planar wall side of the profiled wall cascade. Secondary losses for the profiled wall half, however, show negligible change from the planar cascade results. This can be explained by the fact that the increased turning near the profiled wall causes a reduction of the mass flow through this region which results in lower values of mass averaged loss than area averaged loss.

An understanding of secondary flows and the availability of reliable prediction methods are crucial for the design of low aspect ratio configurations. Unfortunately, the endwall region flow is extremely complicated as is shown to some

Table 2 Loss measurements

	Planar wall cascade					
	Mass averaged			Area averaged		
% span $\Delta P_T/P_T$	0-50	50-100	0-100	0-50	50-100	0-100
Total	0.022	0.025	0.023	0.027	0.032	0.030
Profile	0.011	0.011	0.011	0.012	0.012	0.012
Secondary	0.012	0.014	0.013	0.016	0.020	0.018
	Profiled wall cascade					
% span $\Delta P_T/P_T$	0-50	50-100[a]	0-100	0-50	50-100	0-100
Total	0.018	0.021	0.019	0.021	0.030	0.026
Profile	0.010	0.010	0.010	0.012	0.012	0.012
Secondary	0.007	0.011	0.009	0.010	0.019	0.014

[a] Profiled wall side.

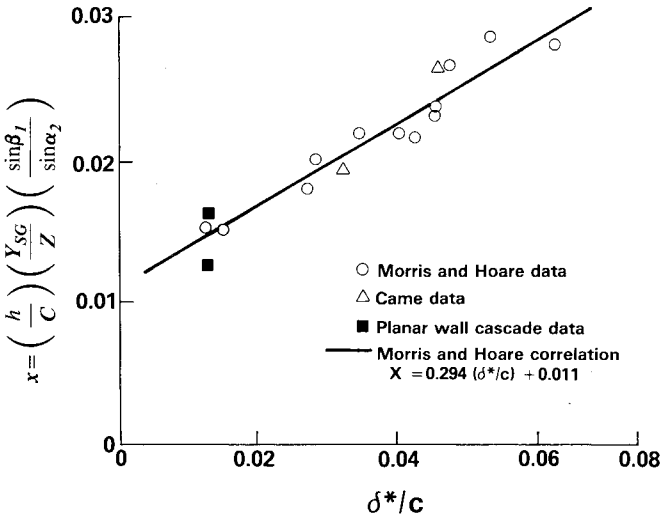

Fig. 10 Comparison of planar wall cascade data with the correlation of Morris and Hoare.

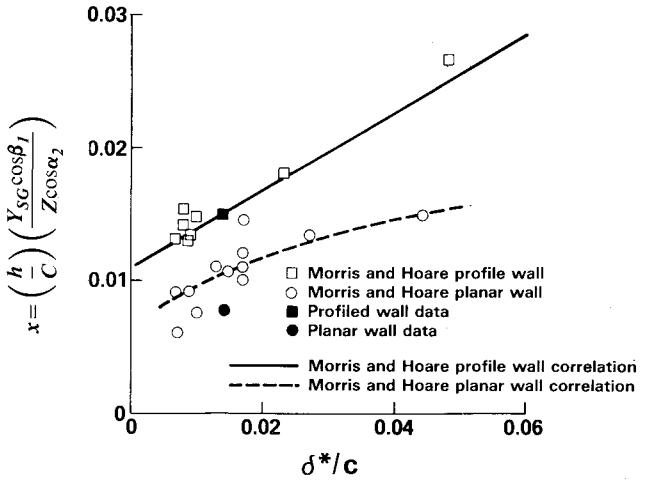

Fig. 11 Comparison of profiled wall cascade data with the Profile A correlation of Morris and Hoare.

degree by the flow visualizations previously discussed. As a consequence, prediction of cascade secondary loss is, for the most part, limited to empirical correlations of experimental data.

Morris and Hoare obtained secondary loss data for a planar wall cascade of inlet guide vanes of 65 deg of gas turning. Their data, along with the data of Came[18] for the same configuration, are presented in Fig. 10 in terms of the resulting correlation. While the Morris and Hoare results are reported to be mass averaged, without local angles and velocities being obtained, the data would in reality reflect more of an area averaging. For this reason, the current area averaged data have been presented in Fig. 10 and are seen to show good agreement.

The secondary loss results obtained for the profiled wall cascade are presented in Fig. 11 along with the data of Morris and Hoare for their "Profile A" configuration, which is very similar to the current profile contour. Here again, area averaged losses have been reported for reasons previously discussed. Also shown in Fig. 11 are the correlations developed for this particular endwall geometry. From this figure it can be seen that the current data fall within the scatter band of the Morris and Hoare data.

An explanation of the above experimental results can best be made in terms of the endwall pressure distributions (loading). In comparing the loading on the planar endwall of the profiled cascade (Fig. 5a) with the loading on endwalls of the planar cascade (Fig. 4), two things are apparent. For one, the profiled cascade endwall is more lightly loaded; and two, the center of pressure is located further aft. These factors contribute to a reduction in the cross passage pressure gradient which serves to misdirect the endwall boundary-layer flow and would suggest a reason for the relative secondary loss performance.

A comparison between the loadings of the profiled endwall of the profiled cascade (Fig. 5d) and the planar endwall cascade (Fig. 4) also shows the profiled endwall to be more lightly loaded again suggesting improved performance, which is consistent with the data. Here the relatively smaller improvement achieved for the profiled wall side is attributed for the most part to the fact that, while the loading is reduced, the maximum Mach numbers for the two endwalls are approximately equal with the profiled endwall being predicted to have a steeper recompression. It should also be noted that the profiled endwall has a slightly larger wetted surface.

Concluding Remarks

The main objective of the cascade test program conducted was to determine the benefit of endwall profiling for a specific low aspect ratio nozzle guide vane configuration. A secondary objective was to examine a range of analytical methods which could be employed in executing future vane designs.

The results obtained for the profiled wall cascade demonstrated a 17% reduction of the full passage mass averaged loss relative to the planar endwall configuration. A major part of the improvement achieved resulted from a reduction of the secondary loss on the planar wall side of the cascade. The secondary loss correlation of Morris and Hoare was found to yield a reasonably good prediction of the area averaged data. The fact that area averaging typically overestimates shear flow loss, as was found to be the case for the current results, suggests that the Morris and Hoare correlation can be used to make conservative secondary loss estimates for design purposes.

Airfoil and endwall static pressure data obtained for the planar wall cascade were very well predicted by the two-dimensional potential flow computation method of Caspar et al. Static pressure data for the profiled wall cascade were well predicted by Denton's three-dimensional time-marching method. This substantiates their suitability for executing design predictions for highly convergent nozzle passages where the regions of flow dominated by viscous effects remain relatively small.

The measured midspan total pressure loss for the planar wall cascade, which should be a good approximation of the two-dimensional performance of the vane section, was well predicted employing boundary layer and control volume wake mixing methods. A prediction for the nearly two-dimensional midspan region of the profiled wall cascade was also in good agreement with the data. Executing profile performance calculations for the turbine component, however, would require accounting for the boundary-layer tripping effects of film cooling arrays and the associated coolant mixing losses.

Surface flow visualizations conducted for the two cascade configurations tested provided qualitative data permitting a degree of understanding of the complex flowfield found in the cascade endwall regions. This understanding allows engineering judgments to be made regarding the anticipated behavior for an annular cascade configuration in addition to providing guidance for executing a film cooled design for high cycle temperature applications.

Acknowledgment

This work was funded by the NASA Lewis Research Center, under the Energy Efficient Engine Component Development and Integration Program, Contract NAS3-20646.

References

[1] Deich, M. E., Zaryankin, A. E., Fillipov, G. A., and Zatsepin, M. F., "Method of Increasing the Efficiency of Turbine Stages with Short Blades," *Teploenergetika,* Vol. 2, Feb. 1960, pp. 240-254.

[2] Ewen, J. S., Huber, F. W., and Mitchell, J. P., "Investigation of the Aerodynamic Performance of Small Axial Turbines," ASME Paper 73-GT-3, Washington, D. C., April 1973.

[3] Morris, A. W. H. and Hoare, R. G., "Secondary Loss Measurements in a Cascade of Turbine Blades with Meridional Wall Profiling," ASME Paper 75-WA/GT-13, Houston, Texas, Nov. 1975.

[4] Baines, W. D. and Peterson, E. G., "An Investigation of Flow Through Screens," *Transactions of ASME,* Vol. 73, July 1951, pp. 467-480.

[5] Batchelor, G. K., *The Theory of Homogeneous Turbulence,* Cambridge University Press, London, 1953, p. 68.

[6] Schlichting, H., *Boundary Layer Theory,* 6th ed., McGraw Hill, New York, 1968, pp. 596-606.

[7] Langston, L. S., Nice, M. L., and Hooper, R. M., "Three-Dimensional Flow Within a Turbine Cascade Passage," *Journal of Engineering for Power, Transactions of ASME,* Vol. 99, Jan. 1977, pp. 21-28.

[8] Carrick, H. B., "Secondary Flow and Losses in Turbine Cascades with Inlet Skew," Cambridge University, Thesis, 1975.

[9] Marchal, P. H. and Sieverding, C. H., "Secondary Losses within Turbomachinery Bladings," AGARD CP 214, 1977.

[10] Caspar, J. C., Hobbs, D. E., and Davis, R. L., "The Calculation of Two-Dimensional Compressible Potential Flow in Cascades Using Finite Area Techniques," *AIAA Journal,* Vol. 18, Jan. 1980, pp. 103-109.

[11] Denton, J. D., "A Time Marching Method for Two and Three-Dimensional Blade-to-Blade Flows," ARC Rept. R&M 3775, 1974.

[12] Denton, J. D., "Extension of the Finite Area Time Marching Method to Three Dimensions," *VKI Lecture Series 84 - Transonic Flow in Axial Turbomachinery,* 1976.

[13] McNally, W. E., "Fortran Program for Calculating Compressible Laminar and Turbulent Boundary Layers in Arbitrary Pressure Gradients," NASA TN D-5681, May 1970.

[14] Cohen, C. B. and Reshotko, E., "The Compressible Laminar Boundary Layer with Heat Transfer and Arbitrary Pressure Gradient," NACA Rept. No. 1294, 1956.

[15] Sasman, P. and Cresci, R., "Compressible Turbulent Boundary Layers with Pressure Gradient and Heat Transfer," *AIAA Journal,* Vol. 4, Jan. 1966, pp. 19-25.

[16] Stewart, W. L., "Analysis of Two-Dimensional Compressible Flow Loss Characteristics Downstream of Turbomachine Blade Rows in Terms of Basic Boundary Layer Characteristics," NASA TN 3515, July 1955.

[17] Amecke, J., "Anwendung der Transsonishen Ähnlichkeitsregel auf die Strömung durch ebene Schaufelgitter," VDI-Forschungsheft 540, 1970.

[18] Came, P. M., "Secondary Loss Measurements in a Cascade of Turbine Blades," *Heat and Fluid Flow in Steam and Gas Turbine Plant,* Institute of Mechanical Engineers Conference Publ. No. 3, Warwick, 1973.